Frictional melting during seismic rupture? A new Raman Spectroscopy approach to detect short-lived heat pulses

Benjamin Moris-Muttoni [1,*]

[*]*benjamin.moris-muttoni@cnrs-orleans.fr*

Co-authors: H. Raimbourg[1], R. Augier[1], A. Canizarès[2], Y. Chen[1]

[1] *Institut des Sciences de la Terre d'Orléans, Université d'Orléans, CNRS, BRGM, ISTO, UMR 7327, F-45071 Orléans, France.*

[2] *CEMHTI-CRNS, UPR 3079, Orléans, France*

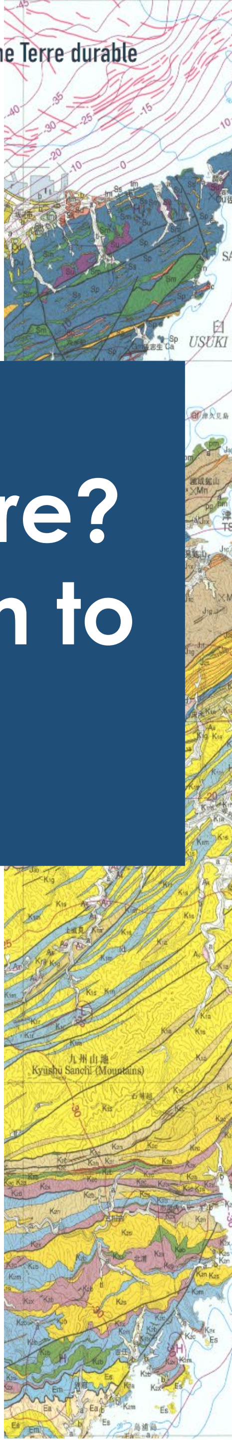

EGU22 – 23rd of May 2022

Introduction – Slip weakening processes in accretionary complexes?

Lubrication by frictional melting has been proposed to be one of the major slip weakening process in crystalline rocks

⮡ Pseudotachylyte veins

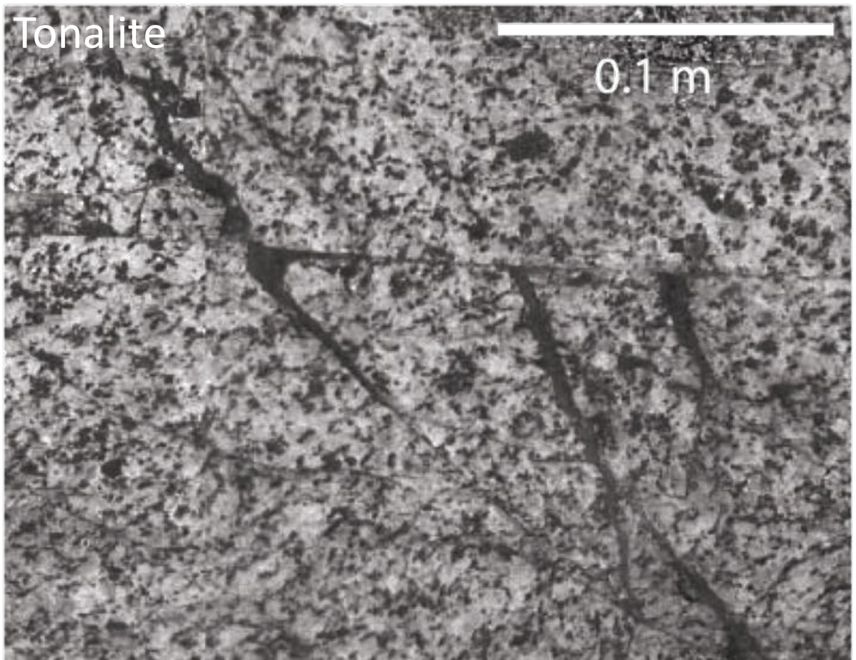

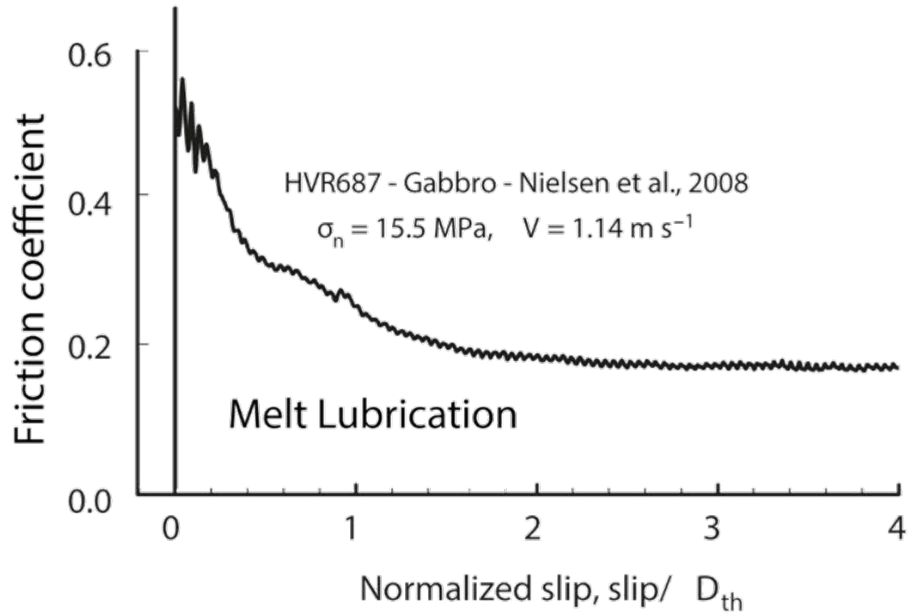

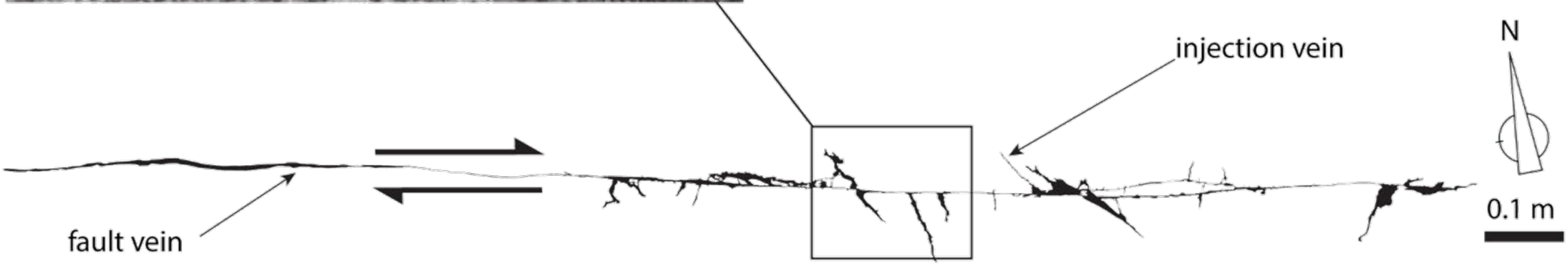

Modified from Di Toro et al., 2006 and Di Toro et al., 2011

Introduction – Slip weakening processes in accretionary complexes?

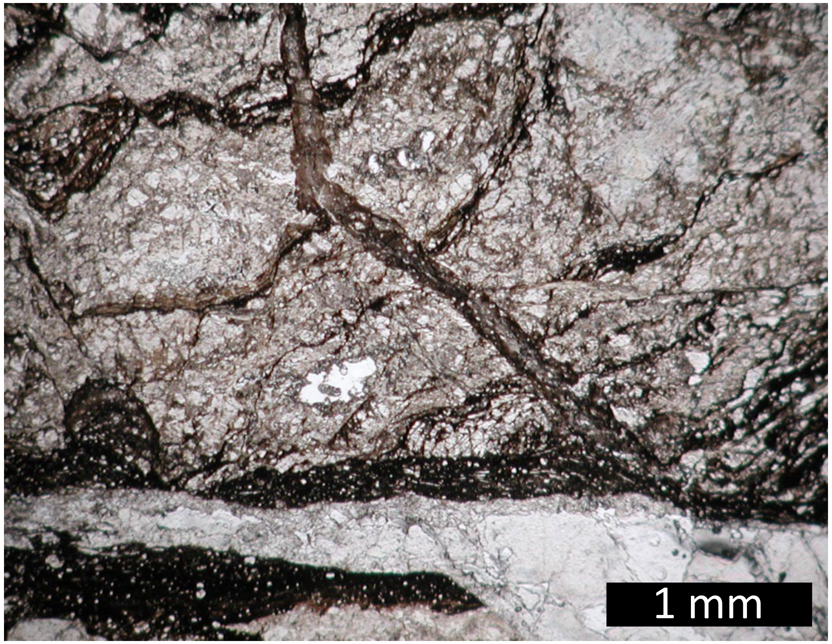

In accretionary complexes, fault core melting is disputable and fault lubrication may be related to other melt-absent processes.

↳ Black Fault Rocks (BFR)

Is frictional heating/melting detectable in accretionary complex rocks ?

Modified from Ujiie et al., 2007

Introduction – Anomalous signal records in natural and exp. BFR

Biomarker thermal maturity

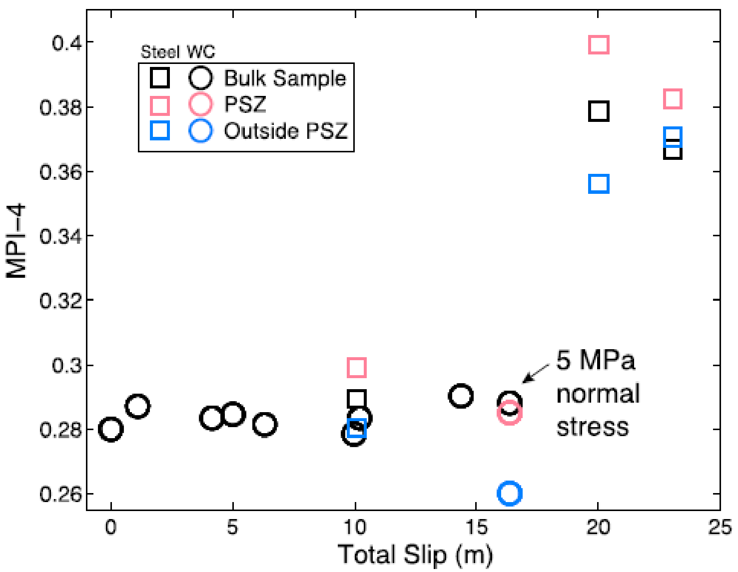

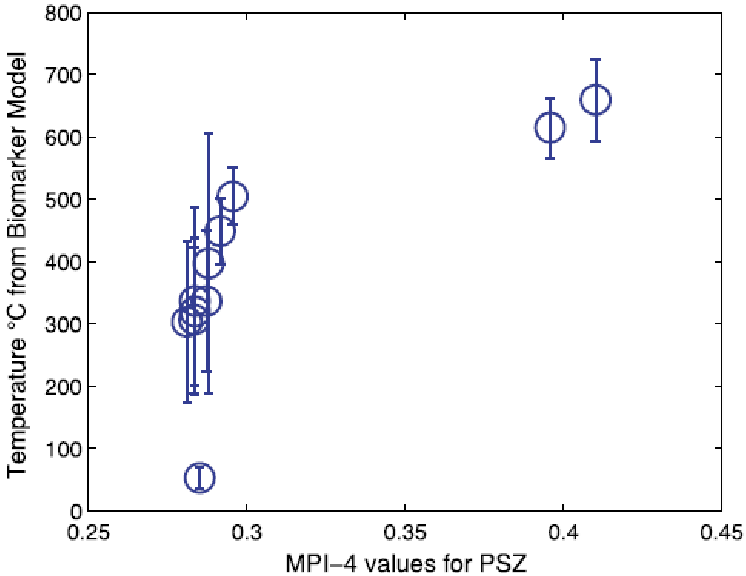

From Savage et al., 2018

InfraRed Spectroscopy of CM

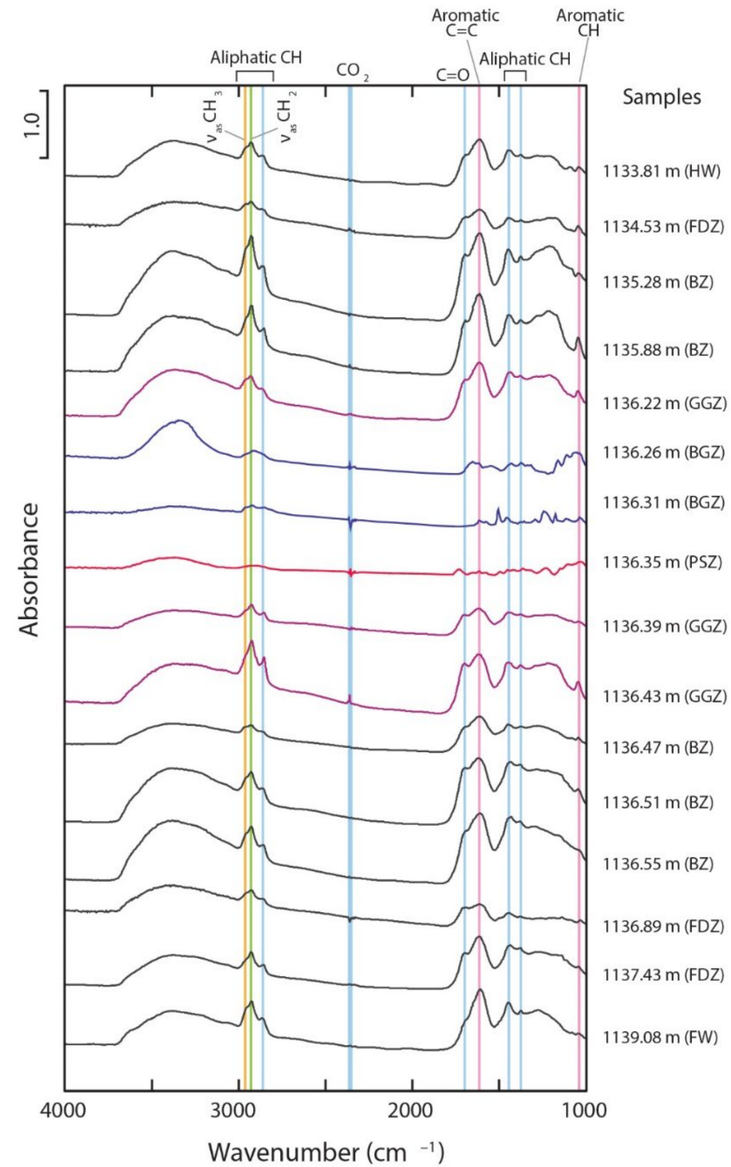

From Hirono et al., 2015

Introduction – Anomalous signal records in natural and exp. BFR

Biomarker thermal maturity

InfraRed Spectroscopy of CM

↳ Lack of spatial resolution using these methods

Raman Spectroscopy of Carbonaceous Materials (RSCM)

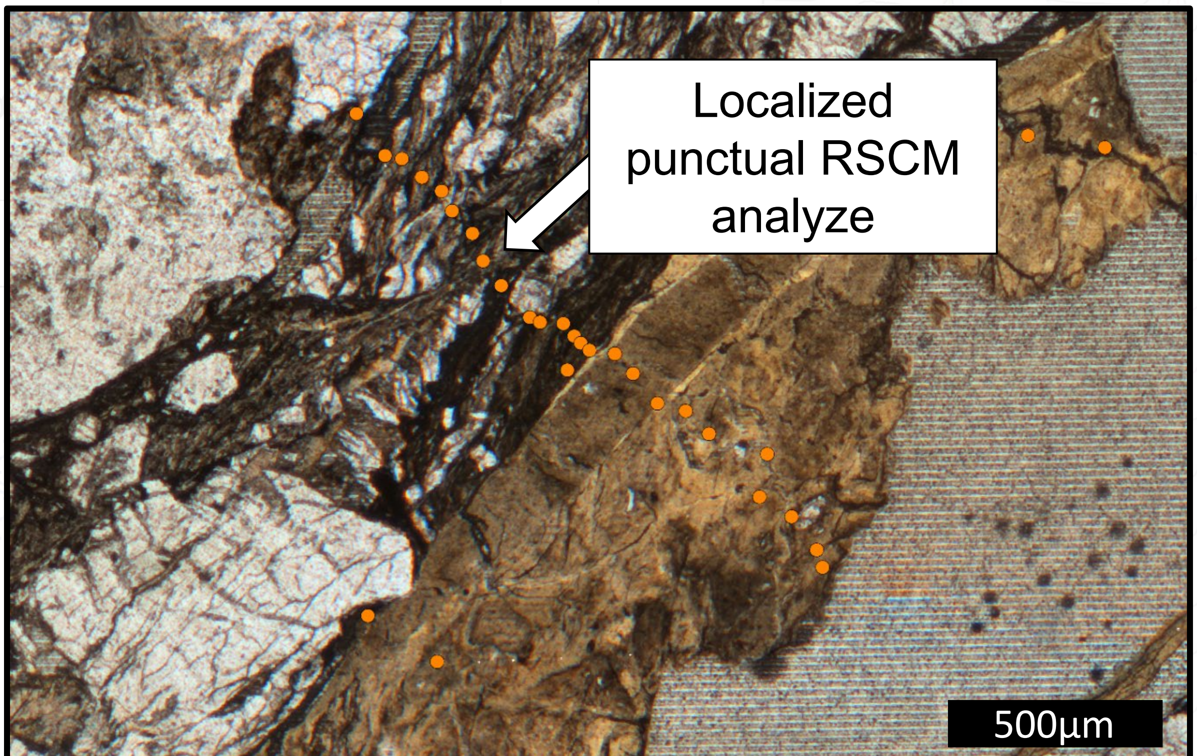

From Savage et al., 2018

From Hirono et al., 2015

Introduction – Anomalous signal records in natural and exp. BFR

Raman Spectroscopy of Carbonaceous Material

Host-rock

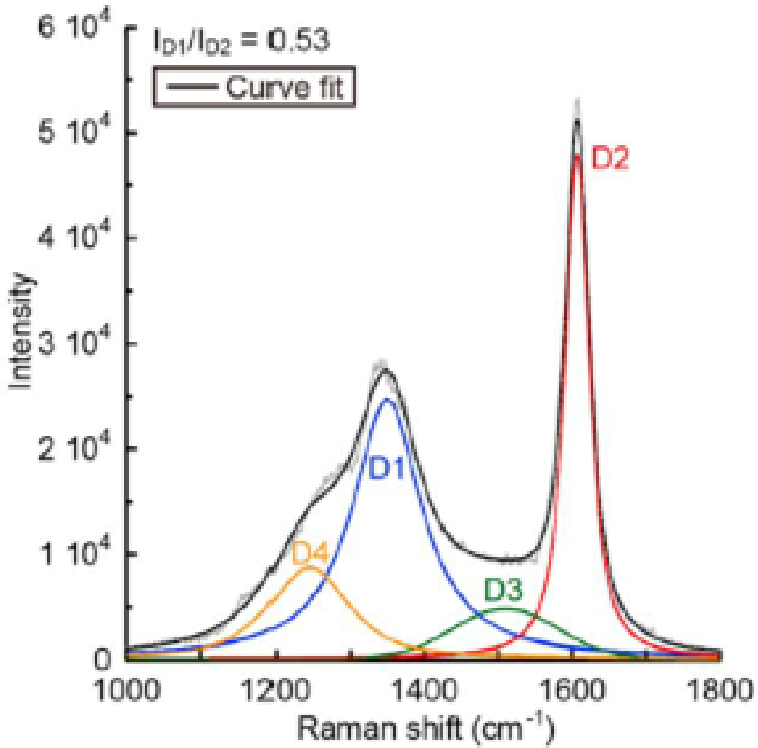

BFR

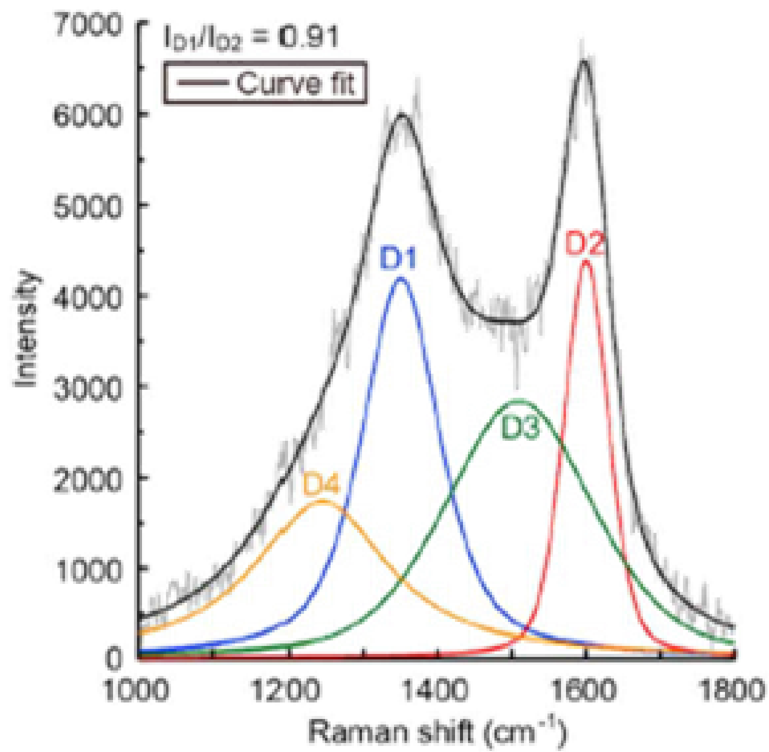

From Ito et al., 2017

Introduction – Anomalous signal records in natural and exp. BFR

Raman Spectroscopy of Carbonaceous Material

Host-rock

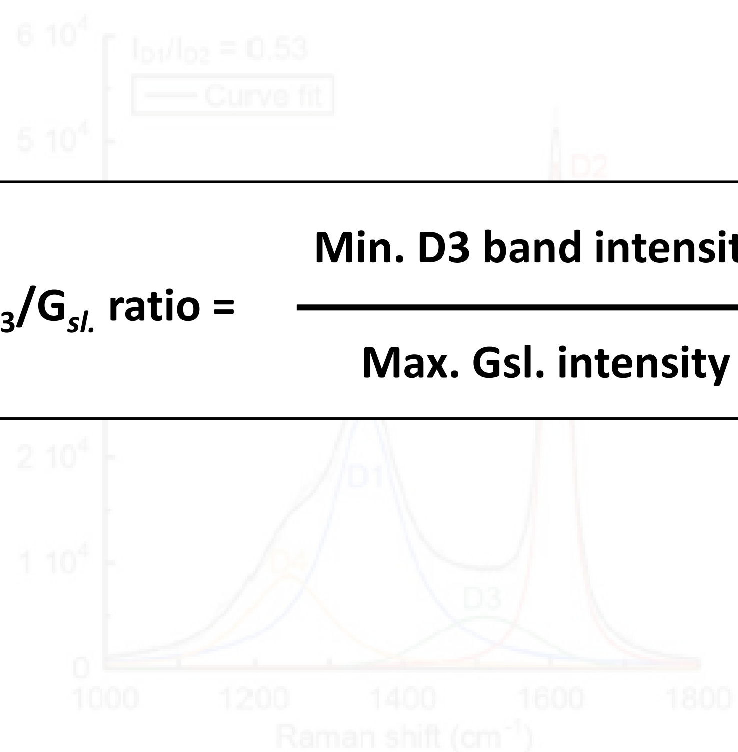

$$D_3/G_{sl.}\ \text{ratio} = \frac{\textbf{Min. D3 band intensity}}{\textbf{Max. Gsl. intensity}}$$

BFR

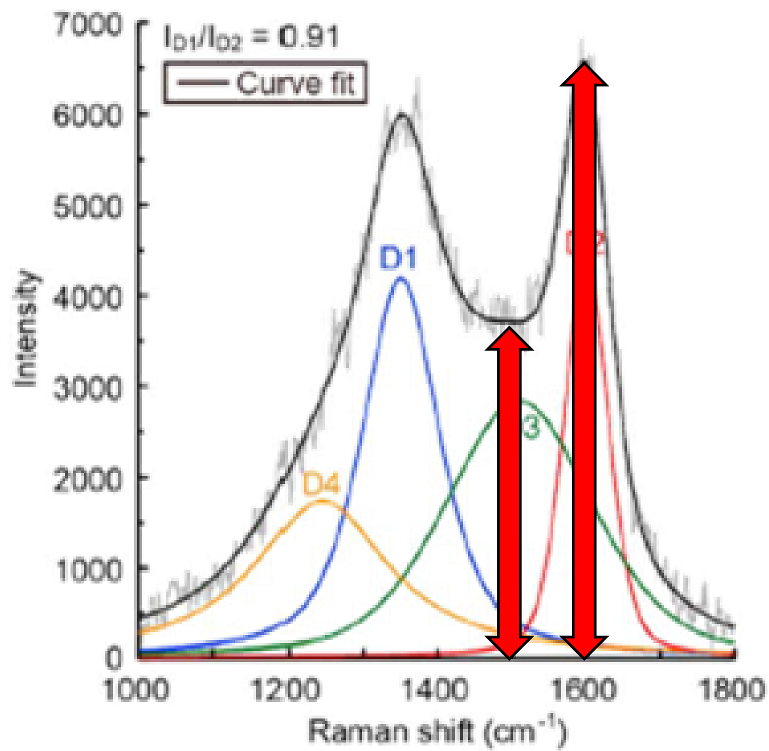

From Ito et al., 2017

- Atypical Raman spectrum shape with high amplitude of the D_3 band
- Establishment of the new Raman parameter $D_3/G_{sl.}$ ratio

Introduction – Anomalous signal records in natural and exp. BFR

Raman Spectroscopy of Carbonaceous Material – Intensity Ratio

Host-rock

BFR

(1) Large dataset from experiments on carbonaceous matter-bearing rocks (HFV, Stick-Slip, Pyrolysis) help to discriminate the short-lived intense temperature effects on RSCM signal

(2) New experiments of laser heating on natural sediments: “Flash-heating experiment”

Highlight the short-lived intense heating on RSCM signal and unravel the thermal history of fault zones

Thermal and strain effects operate conjointly and both influence the CM crystallinity

Our recent study (Moris-Muttoni et al., 2022) demonstrates the major control of strain on the intensity ratio

Results – (1) Short-lived intense heating on CM-bearing rocks exp.

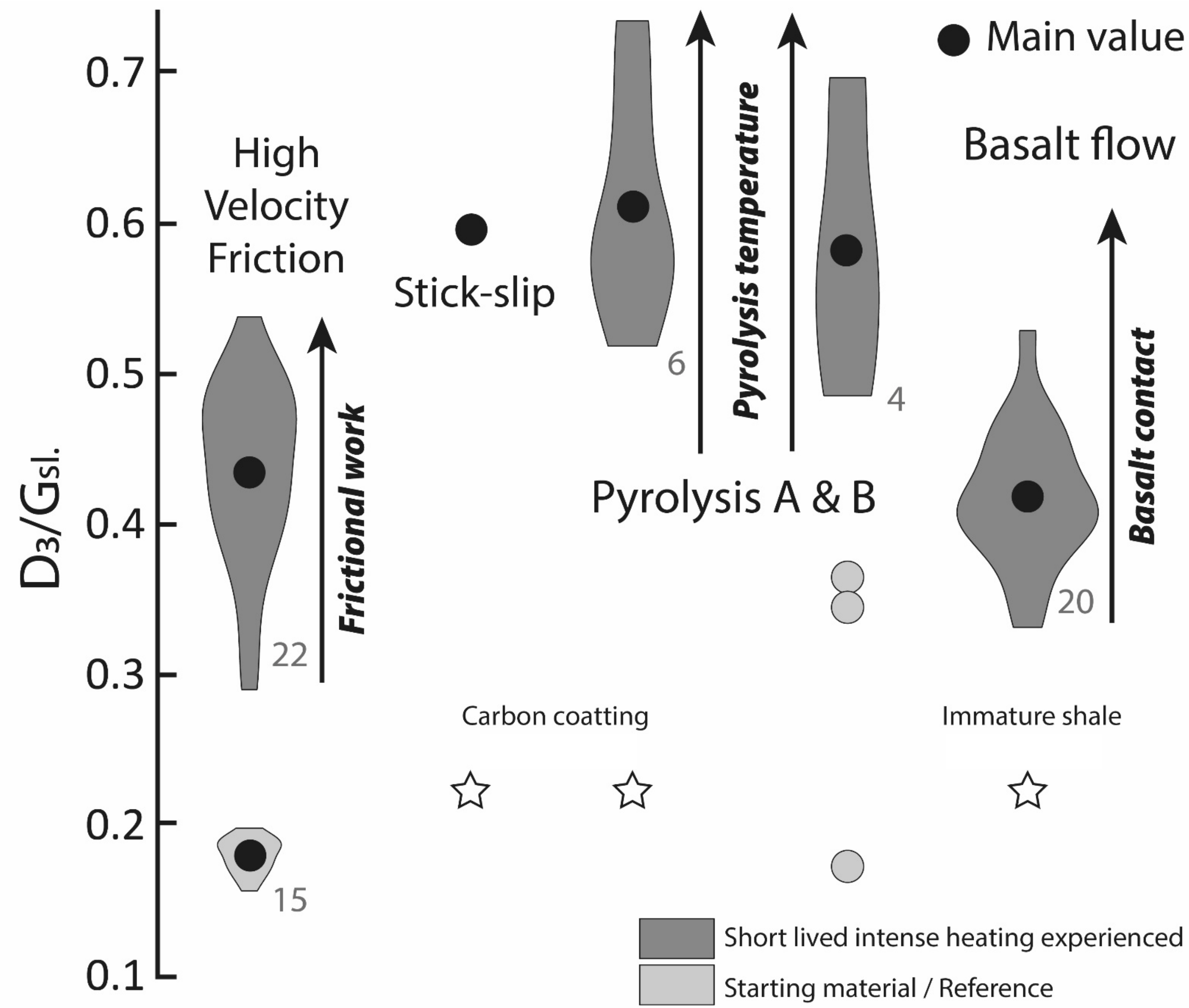

Results – (2) Flash-heating experiments

Flash-heating experiments to simulate intense and short-lived heating without any strain

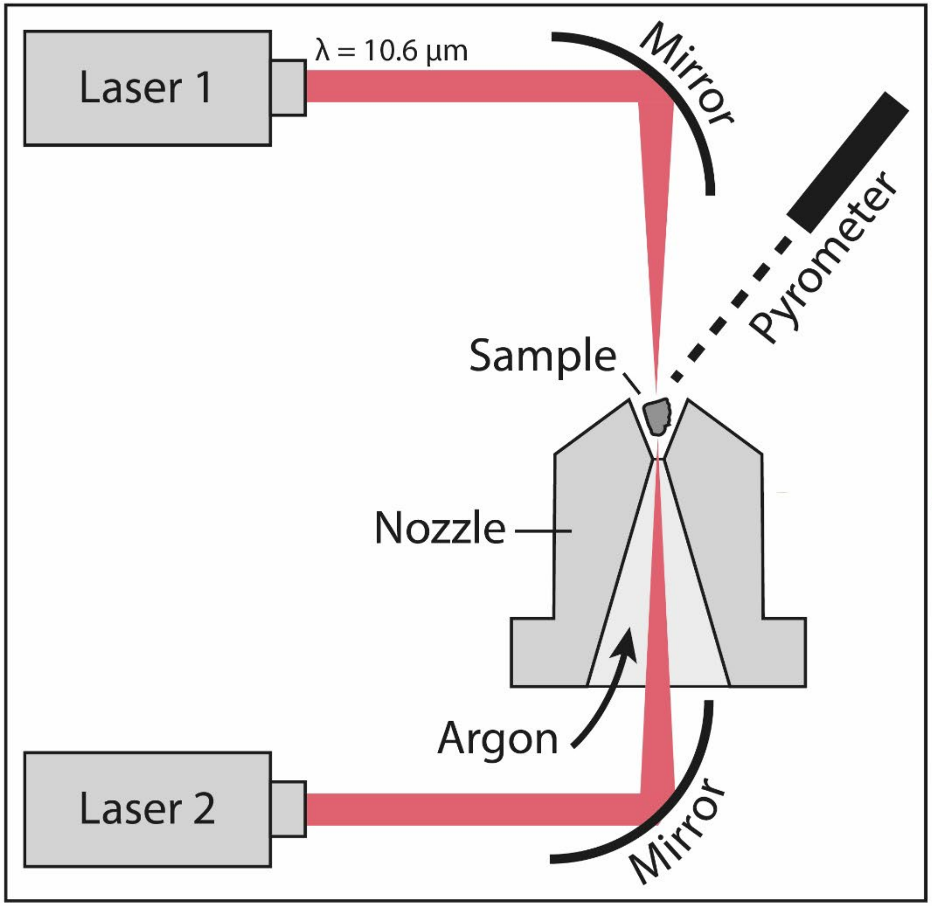

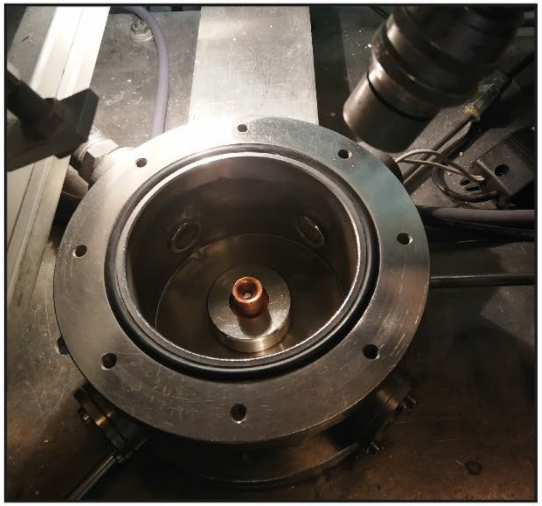

Starting material :
pre-matured shale (ca. 200°C)

Under Argon flow

Exposure: 0.5 to 60 seconds

Estimated temperature: ca. 1400°C

Results – (2) Flash-heating experiments

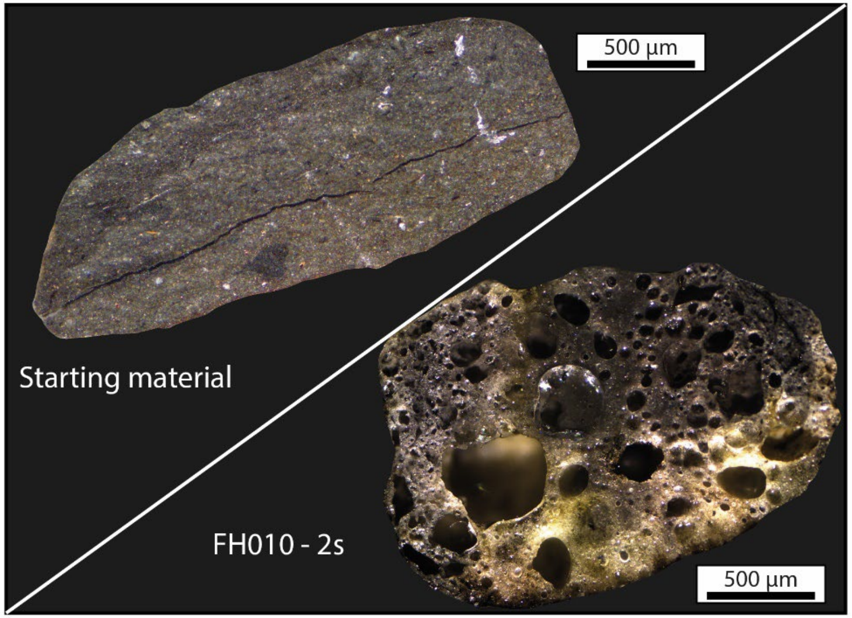

Flash-heated samples become spherical and degazing pores appear, grow and collapse

Results – (2) Flash-heating experiments

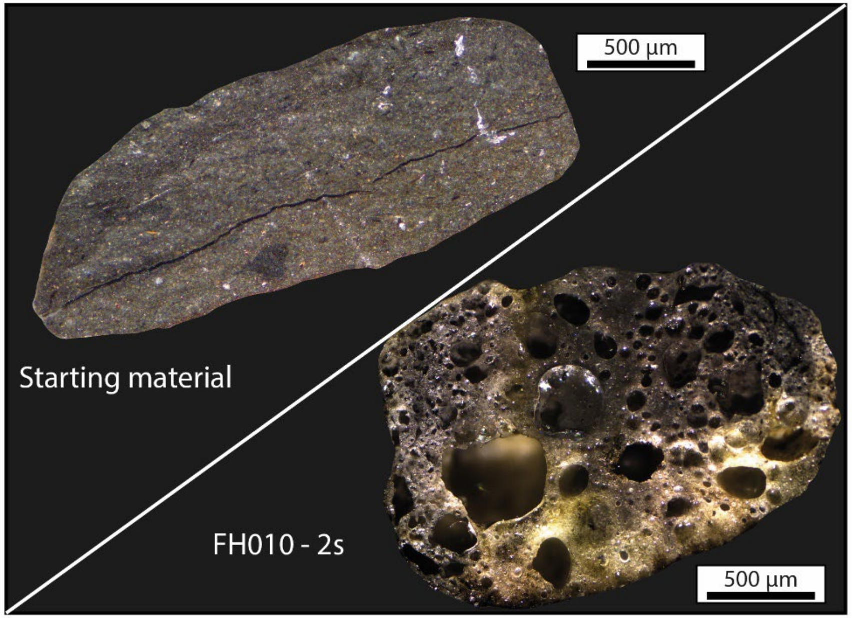

Atypical Raman spectrum shape is observed

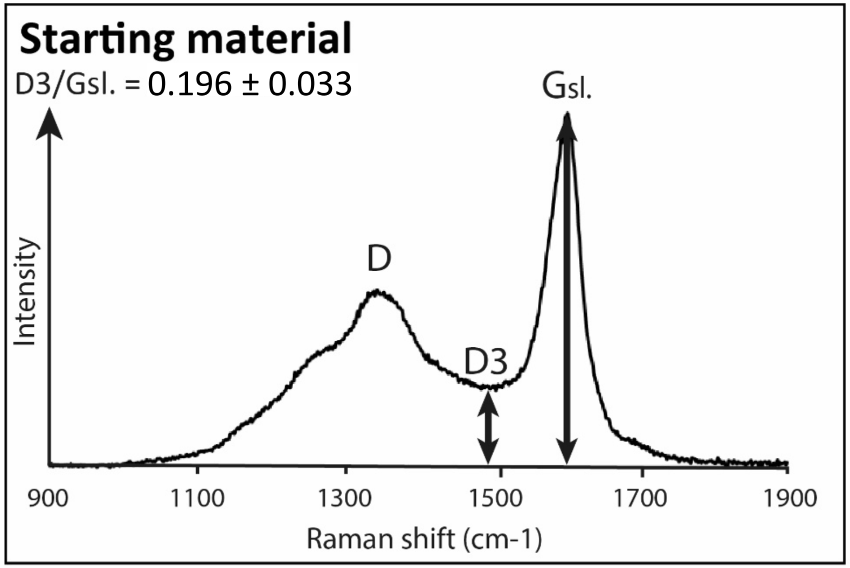

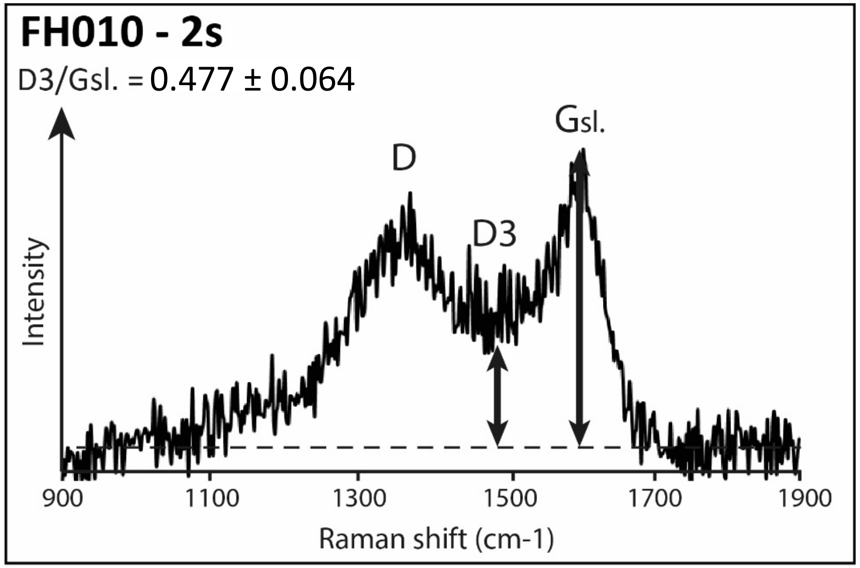

Results – (2) Flash-heating experiments

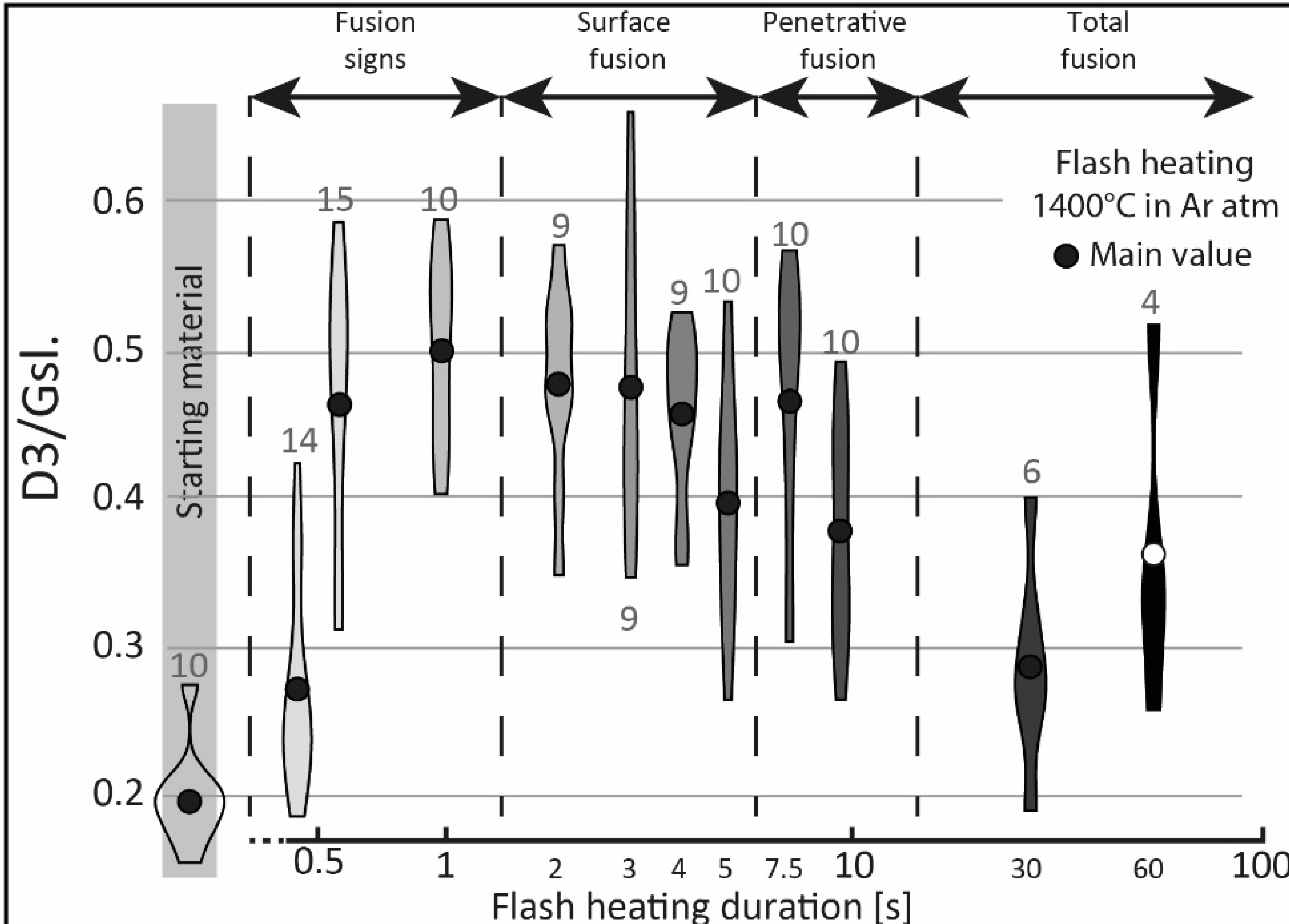

Results – (2) Flash-heating experiments

Strong sensitivity of the $D_3/G_{sl.}$ ratio to the short-lived intense heating

Samples that experienced flash-heating show $D_3/G_{sl.}$ ratio up to 0.6

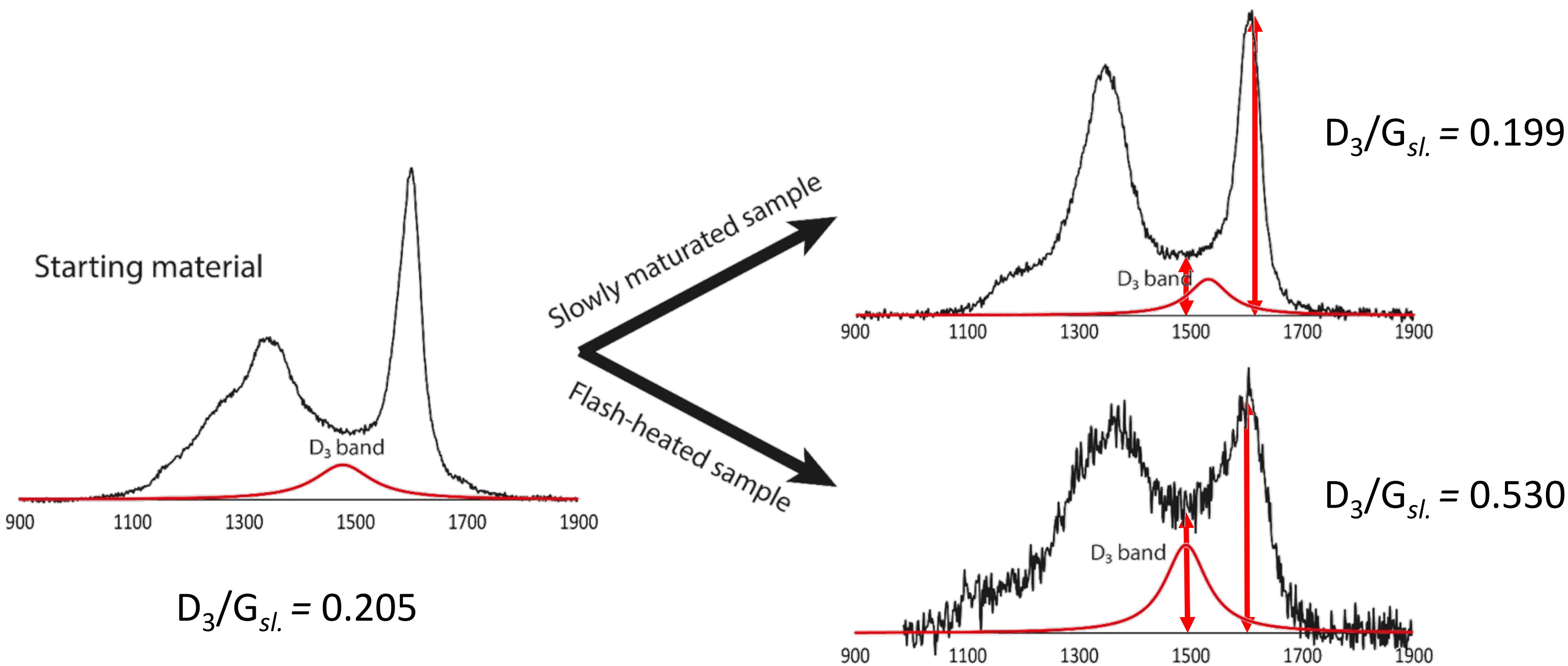

Results – Application to natural fault cores: Geological settings

5 Black Fault Rocks interpreted as quenched melts veins by frictional heating

Mugi BFR

Kure BFR

Okitsu BFR

Nobeoka BFR

— Shimanto Belt, Japan

Kodiak BFR — Kodiak Accretionary Complex, Alaska

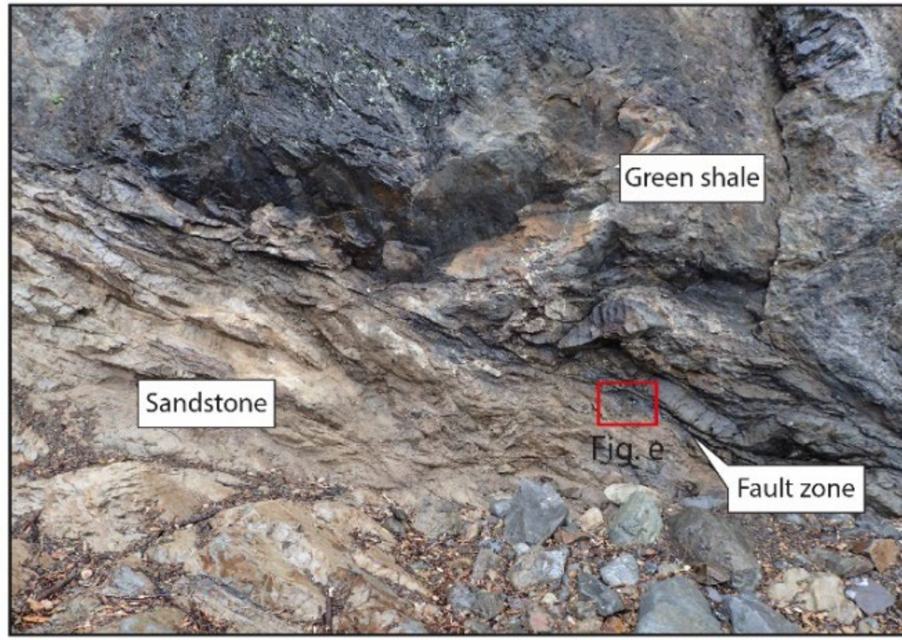

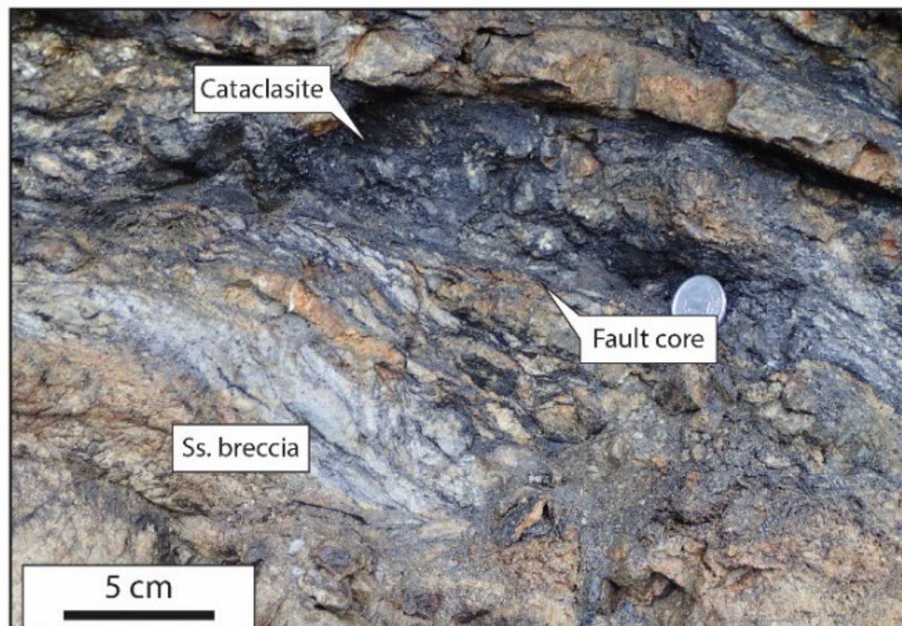

Results – Application to natural fault cores: BFR microstructures

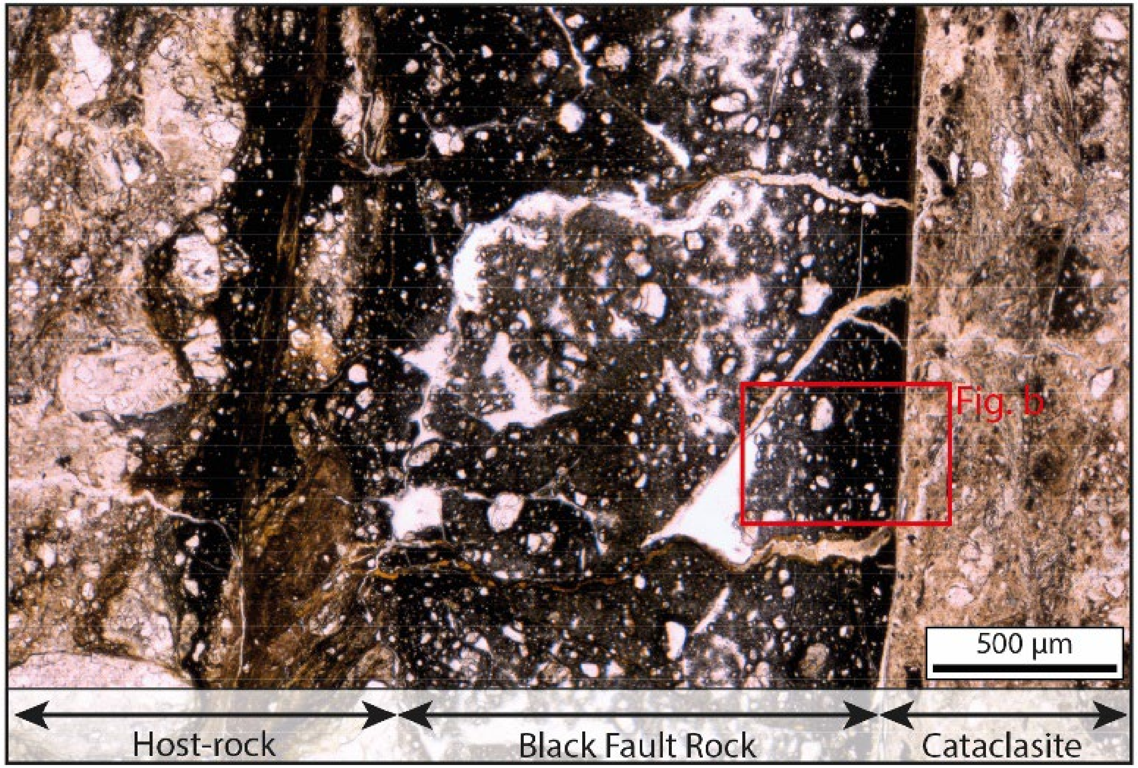

The Kure BFR

1 to 3 mm-thick multi-layering vein cutting across the sandstone-rich host-rock

Results – Application to natural fault cores: BFR microstructures

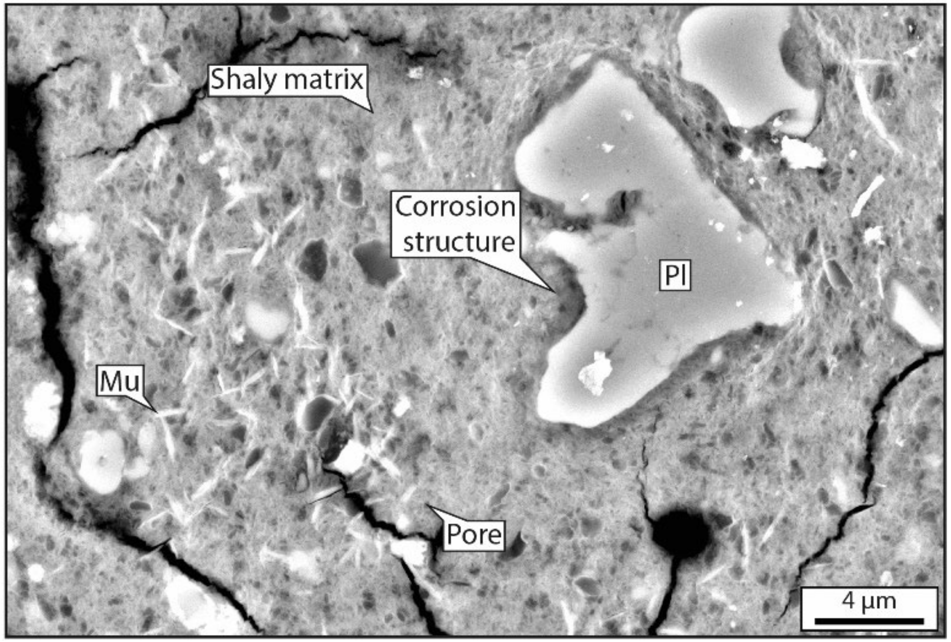

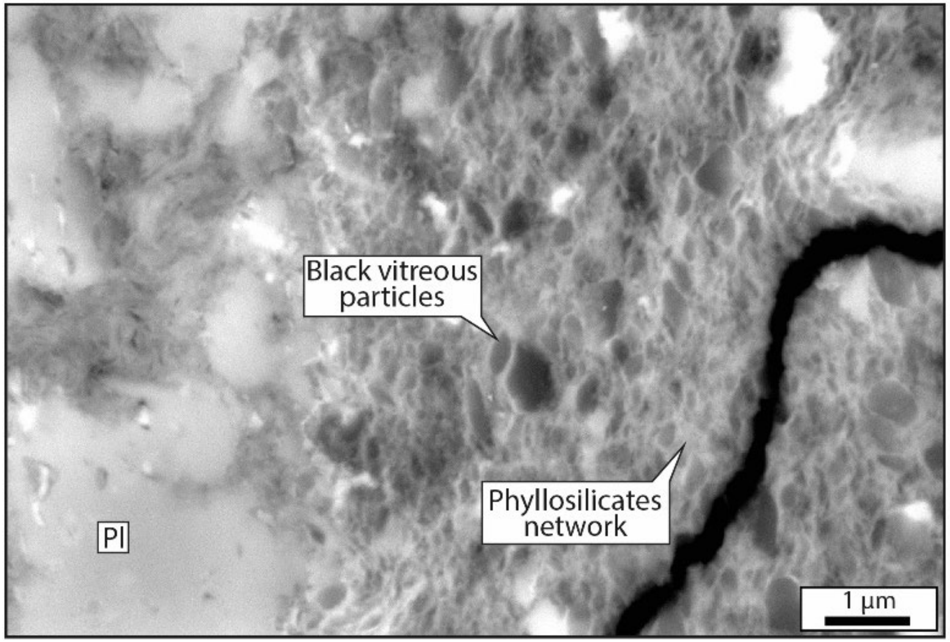

The Kure BFR

Ultra-fine grained shale-rich matrix composed of acicular Muscovites (2 µm) and glassy particles (<1µm)

Embedded corroded albite and quartz clasts (5 to 10µm)

Results – Application to natural fault cores: BFR microstructures

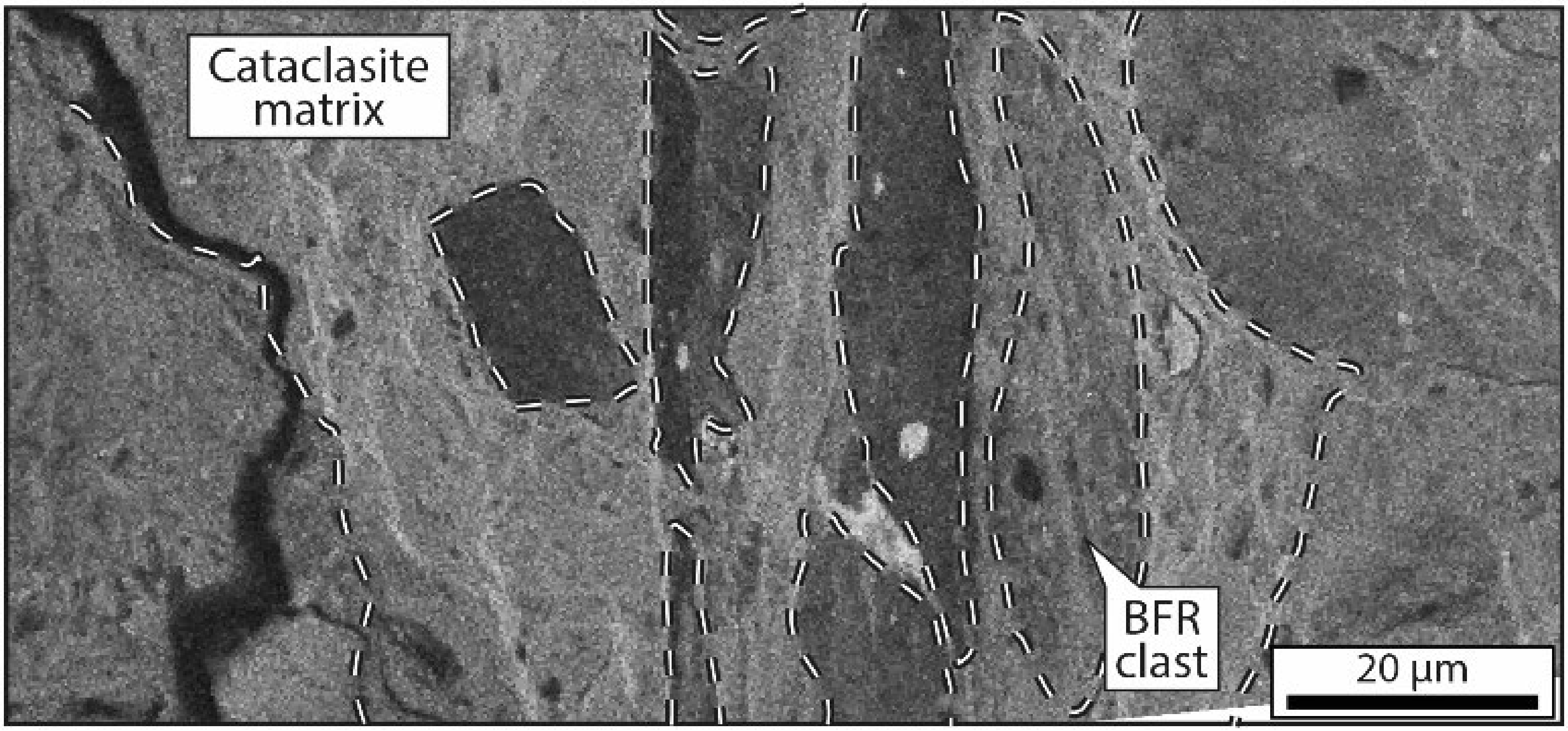

0.5 to 2mm thick cataclasite with scattered porphyroclasts and µm-large BFR clasts embedded in a shaly matrix

Results – Application to natural fault cores: RSCM results

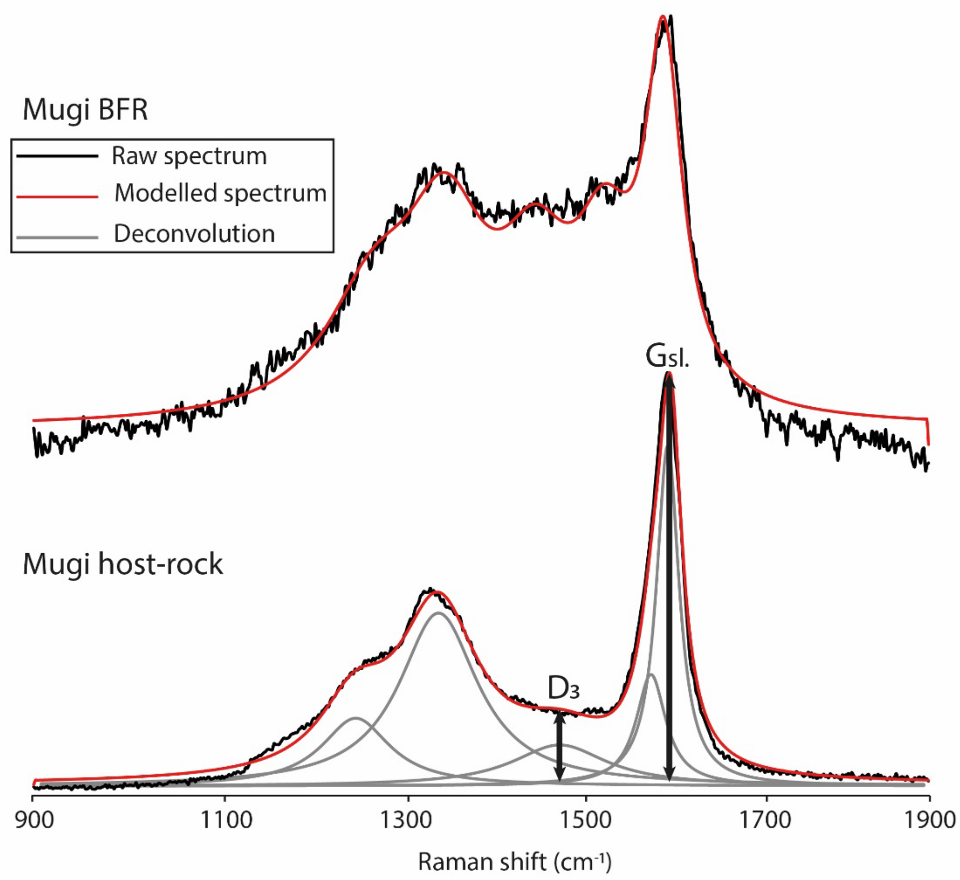

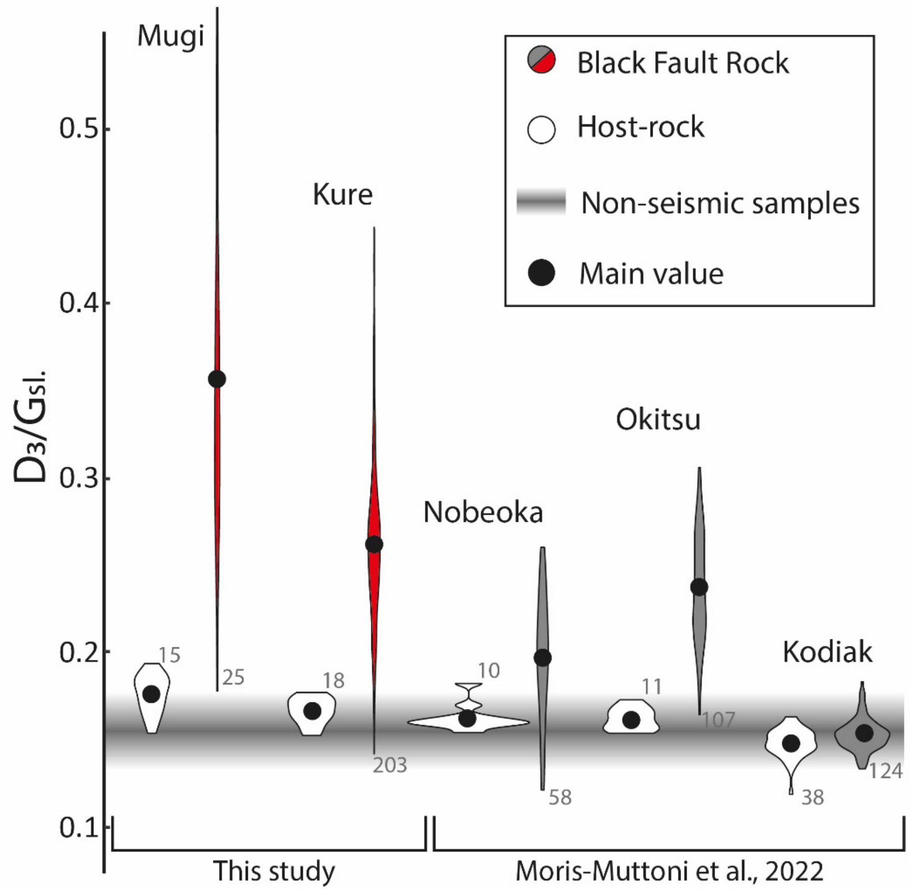

- Atypical Raman spectra in Japanese BFR comparing with HR and metamorphic references
- $D_3/G_{sl.}$ ratio show a large increase and a large dispersion from 0.2 up to 0.6 in Japanese BFR
- In Kodiak BFR $D_3/G_{sl.}$ ratio is similar to the host-rock and metamorphic references

Results – Application to natural fault cores: RSCM/microstructure results

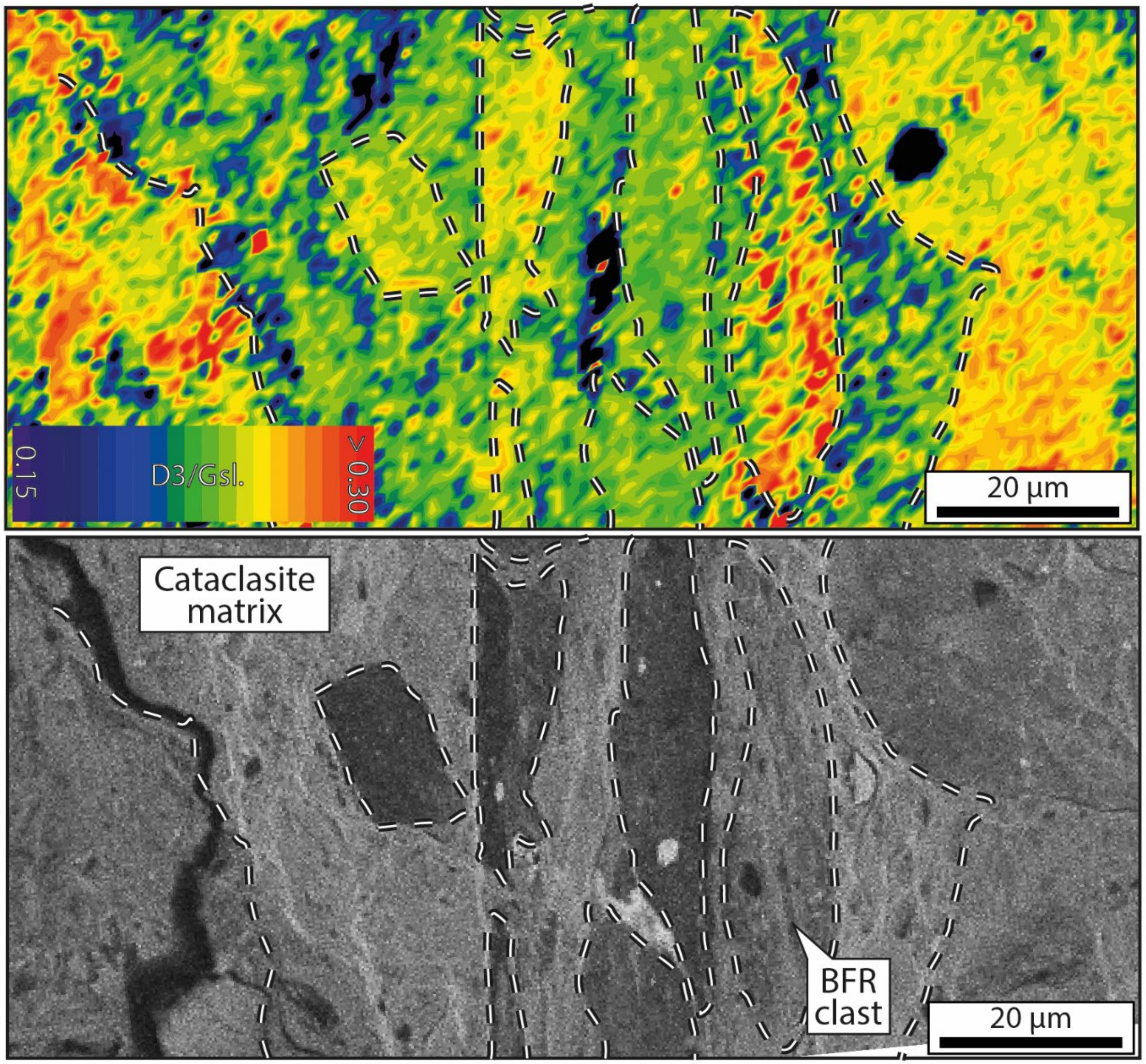

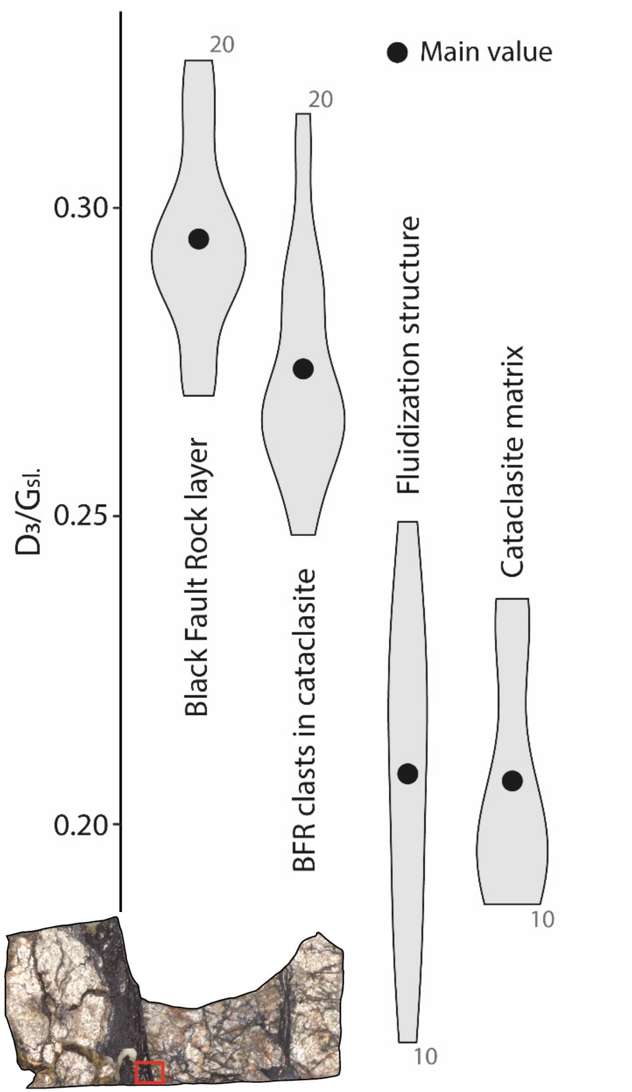

- $D_3/G_{sl.}$ ratio varies as a function of microstructures with increasing values in the BFR clasts embedded in the cataclasite matrix

Conclusion – Interpretation of $D_3/G_{sl.}$ ratio and application

Experimental and natural samples that experienced short-lived intense heating present atypical Raman spectra with high amplitude of the D_3 band and increasing $D_3/G_{sl.}$ ratio

↳ **$D_3/G_{sl.}$ ratio is a reliable tool to highlight the short-lived intense heating**

Kure BFR

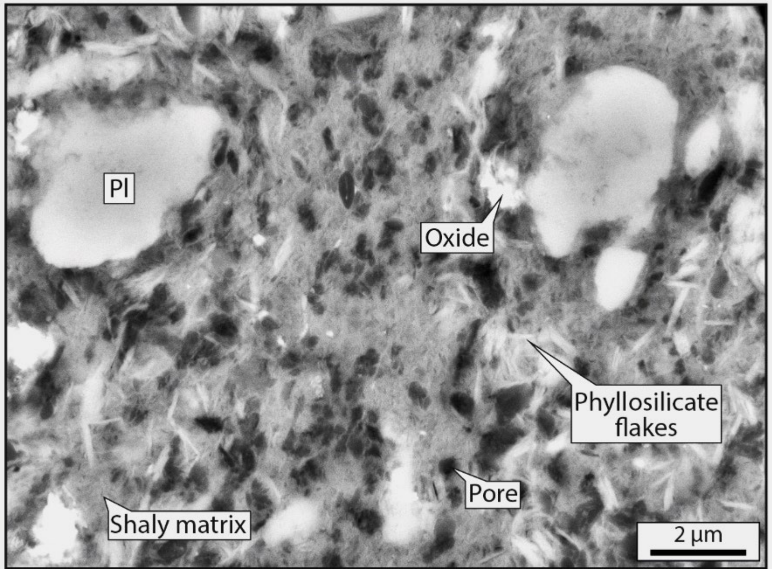

Identical microstructure observations for the 5 BFR independently of the origin

Kodiak BFR shows similar $D_3/G_{sl.}$ ratio to the host-rock, whereas Japanese BFR show increase in the faulted layers compared to the host-rocks

↳ **$D_3/G_{sl.}$ ratio could help to decipher the BFR origin (i.e., Frictional heating vs. Mechanical comminution)**

Kodiak BFR

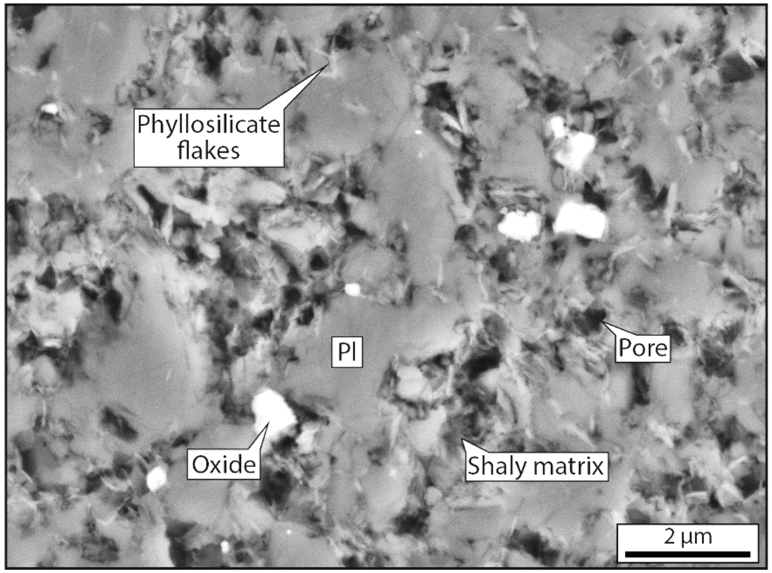

Acknowledgments

We warmly thank our Japanese colleagues, **Pr. Sakaguchi A., Dr. Mukoyoshi H., Dr. Yamaguchi A. and Dr. Ujiie K.** respectively from the University of Yamaguchi, University of Shimane, University of Tokyo and University of Tsukuba for shearing their Black Fault Rocks samples for this study.

This work was supported by the **Institut National des Sciences de l’Univers** financial program

Experimental work was supported thanks to the **LabEx-Voltaire** (LABX-100-01) and **EquipEx PLANEX** (ANR-11-EQPX-0036) programs

Supplementary figures

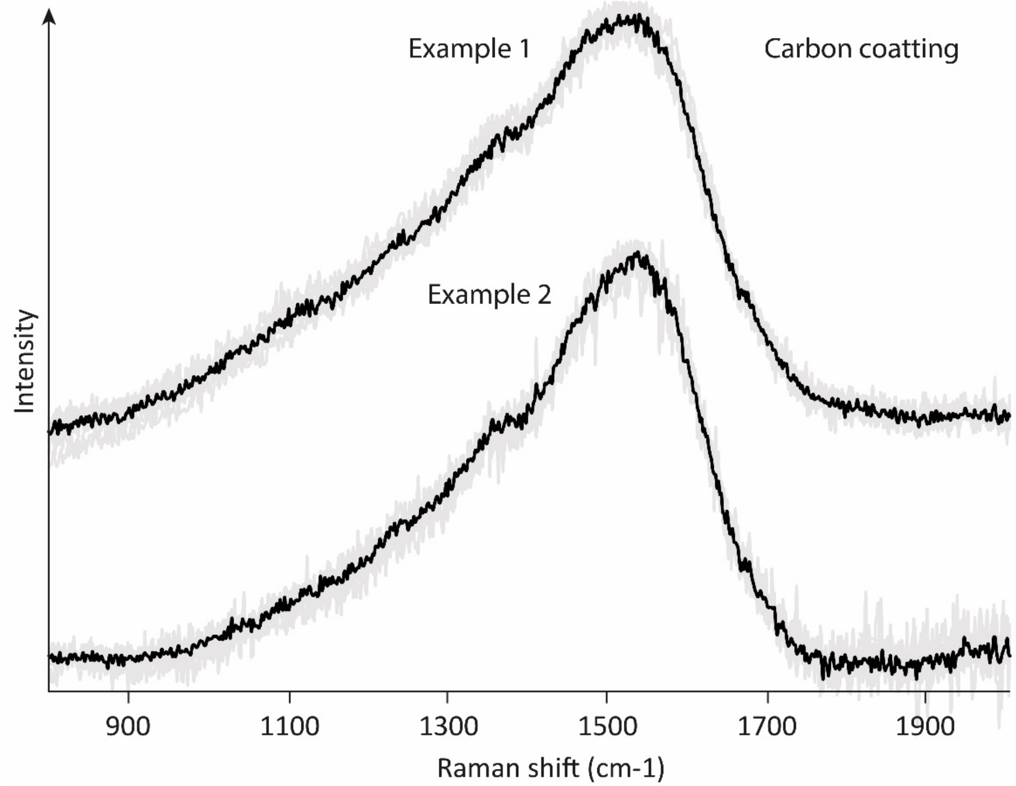

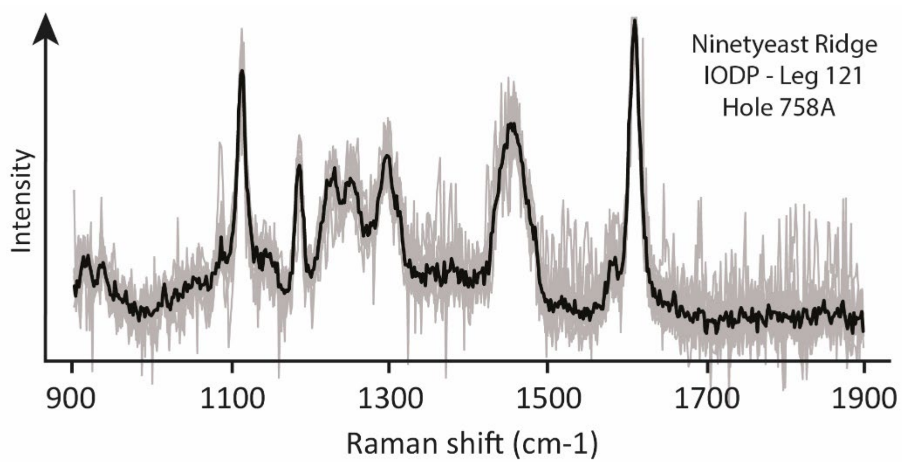

Supplementary figures

				Textures				
Sample	**Location**	**Latitude**	**Longitude**	**Geological unit**	**Fault core width**	**Single/Multi tectonic event**	**Fluidization structure**	**Glassy matrix**
Mugi	Japan	33.685691	134.479710	Mugi mélange	1 mm	Single	Yes	Yes
Kure	Japan	33.307346	133.250186	Kure mélange	1 - 3mm	Single	Yes	Yes

	Micro- to nano-textures									
Sample	**Rounded clasts**	**Clasts grain size**	**Corrosion / Embayment structure**	**Flow texture**	**Matrix grain size**	**Fine-grains within matrix**	**Nature of fine-grains**	**Fine-grains size**	**Pores in the matrix**	**References**
Mugi	Yes	5 - 50 µm	Yes	No	-	Yes	Accicular mullites, Fe-rich, Ti-rich particles	20 - 200 nm and 1 - 10 µm	Yes	Ujiie et al., 2007
Kure	Yes	5 - 10 µm	Yes	No	-	Yes	Acicular muscovites	2 µm	Yes	Mukoyoshi et al., 2006

Supplementary figures

Microstructural zones	Phases	SiO2	TiO2	Al2O3	FeO	MnO	MgO	CaO	Na2O	K2O	Cl	SO2	Total (%)
Porphyroclasts	Plagioclase	69,2320	0,0885	20,4945	0,0558	0,0000	0,0000	0,5794	8,7582	0,2063	0,0000	0,0000	99,4146
		69,1850	0,0000	20,2378	0,0681	0,0505	0,0413	0,2600	9,7354	0,2828	0,0000	0,0135	99,8744
		66,4008	0,1307	19,7350	1,1435	0,1092	0,1316	0,1833	9,5012	0,9287	0,0341	0,0472	98,3454
		67,4761	0,0593	20,3471	0,3130	0,0000	0,1825	0,4739	9,6693	0,5499	0,0012	0,0339	99,1062
		67,8097	0,0000	20,7930	0,8348	0,0034	0,3035	0,5137	9,6100	0,6306	0,0000	0,0000	100,4988
		69,0256	0,0291	19,7466	0,0000	0,0000	0,0057	0,2204	10,9274	0,0345	0,0053	0,0123	100,0070
		67,7604	0,0000	20,0806	0,2102	0,0000	0,0069	0,6124	10,1293	0,2962	0,0000	0,0429	99,1390
		67,7156	0,0000	19,7937	0,0588	0,0554	0,0021	0,8798	10,2021	0,0810	0,0014	0,0000	98,7898
		68,7187	0,0000	19,8588	0,0340	0,0840	0,0390	0,2825	10,5981	0,2263	0,0083	0,0000	99,8497
		69,5944	0,0530	19,2228	0,0000	0,0000	0,0192	0,0222	11,0817	0,0757	0,0000	0,0000	100,0690
		66,3725	0,1398	21,0071	0,1005	0,0403	0,0080	2,1997	9,6628	0,1629	0,0000	0,0000	99,6936
		69,1530	0,0080	19,6959	0,1423	0,0655	0,0000	0,1400	10,6660	0,1953	0,0092	0,0470	100,1221
		67,9412	0,0000	20,4516	0,1144	0,0000	0,0147	0,6366	10,6697	0,2348	0,0000	0,0000	100,0630
		68,6030	0,0265	20,0501	0,1855	0,0000	0,0257	0,6590	10,6823	0,1478	0,0205	0,0000	100,4004
		64,7242	0,1323	20,3952	2,1138	0,0520	0,3085	0,5840	8,4798	1,2629	0,0218	0,0131	98,0874
		68,8060	0,0345	19,6227	0,1251	0,0000	0,0815	0,2327	7,1816	2,0791	0,0000	0,0000	98,1633
	K-feldpsar	65,5405	0,0559	18,1864	0,2350	0,0000	0,0000	0,0000	0,6524	15,2818	0,0000	0,0000	99,9521
BFR matrix	Phyllosilicate-rich zone	41,0273	0,3591	20,5292	9,6374	0,0016	2,1182	1,1858	0,6170	5,3700	0,1869	0,0702	81,1028
		43,3244	0,4335	23,2992	8,9505	0,1350	1,8435	0,9622	0,4744	5,3515	0,1345	0,0500	84,9586
		43,1629	0,3332	21,9477	11,0206	0,1475	1,6181	1,0572	0,4293	5,2811	0,1125	0,0521	85,1621
		44,9058	0,3190	23,8010	6,1254	0,0432	1,7863	0,9964	0,4378	5,5797	0,0829	0,0411	84,1184
		44,8697	0,3310	24,5676	5,4680	0,0696	1,8285	1,1813	0,5372	5,6325	0,0689	0,0729	84,6271
		48,6393	0,2868	26,5693	5,3792	0,0000	2,0617	0,8865	0,4938	5,7698	0,0390	0,0420	90,1674
		49,6410	0,5344	26,7271	4,1857	0,0748	2,0962	0,8368	0,4890	5,8849	0,0709	0,0233	90,5640
		47,5257	0,2739	25,0040	4,6463	0,0382	1,9900	0,7933	0,5739	5,5237	0,0617	0,0508	86,4814
		45,4431	0,6959	24,7687	5,9692	0,0000	3,3870	0,8393	0,4657	5,8006	0,0110	0,0302	87,4105
		44,7751	0,0141	26,4848	2,1004	0,0000	1,9843	0,5595	0,4004	7,1906	0,0456	0,0813	83,6361
		42,9044	0,2291	25,5621	7,0017	0,0000	1,5433	0,1176	0,1619	5,5321	0,2402	0,0433	83,3357
		48,0440	0,5095	27,2153	5,5578	0,0000	2,1726	0,1154	0,1813	7,2686	0,1401	0,0000	91,2047
		45,5163	0,1068	26,6887	5,0198	0,0299	1,9990	0,0796	0,1381	6,0835	0,1808	0,0000	85,8425
		43,7780	2,5494	25,4475	3,0310	0,1600	2,0485	0,2424	0,1753	6,4929	0,1833	0,0647	84,1730
		46,4636	0,1392	28,5992	2,6688	0,0301	1,9415	0,1513	0,2159	6,4646	0,2325	0,0160	86,9226
		40,7055	1,4947	23,1233	2,8780	0,1583	1,8427	2,0409	0,3792	6,3334	0,0377	0,0884	79,0820
	Black clasts-rich zone	30,4676	1,8669	16,7406	10,5590	0,0980	1,0439	0,7082	0,4848	3,6303	0,0792	**0,6358**	66,3143
		31,5526	1,5301	16,9913	7,8925	0,0674	0,9949	0,6934	0,5666	3,6014	0,0784	**0,7302**	64,6988
		38,1102	1,3023	20,9843	4,1724	0,1427	1,4495	0,7095	0,4731	4,6203	0,0664	**0,5296**	72,5603
		45,6456	0,3571	20,0873	4,3118	0,0000	1,2838	0,6965	2,3415	4,7702	0,0518	**0,3891**	79,9346
		37,9076	0,8434	20,3719	5,0068	0,0731	1,6428	0,8462	0,4541	4,5850	0,0629	**0,4444**	72,2380
		31,2119	1,0532	17,0671	3,8524	0,0050	1,0732	0,7621	0,4238	3,9926	0,0900	**0,7536**	60,2849
		34,8894	0,8326	19,5580	3,8227	0,0682	1,1416	0,7281	0,3793	4,5138	0,0624	**0,8116**	66,8075